Effect of Oxalic Acid Concentration and Different Mechanical Pre-treatments on the Production of Cellulose Micro/nanofibers

Gabriela Adriana Bastida
Instituto de Tecnología Celulósica, Facultad de Ingeniería Química (FIQ-CONICET), Universidad Nacional del Litoral

Carla Natalí Schnell
Instituto de Tecnología Celulósica, Facultad de Ingeniería Química (FIQ-CONICET), Universidad Nacional del Litoral

Paulina Mocchiutti
Instituto de Tecnología Celulósica, Facultad de Ingeniería Química (FIQ-CONICET), Universidad Nacional del Litoral

Yamil Nahún Solier
Instituto de Tecnología Celulósica, Facultad de Ingeniería Química (FIQ-CONICET), Universidad Nacional del Litoral

María Cristina Inalbon
Instituto de Tecnología Celulósica, Facultad de Ingeniería Química (FIQ-CONICET), Universidad Nacional del Litoral

Miguel Ángel Zanuttini
Instituto de Tecnología Celulósica, Facultad de Ingeniería Química (FIQ-CONICET), Universidad Nacional del Litoral

María Verónica Galván (vgalvan@fiq.unl.edu.ar)
Instituto de Tecnología Celulósica, Facultad de Ingeniería Química (FIQ-CONICET), Universidad Nacional del Litoral

Research Article

Keywords: oxalic acid, refining, rotary homogenizer, intrinsic viscosity, aspect ratio, sedimentation

Posted Date: June 17th, 2022

DOI: https://doi.org/10.21203/rs.3.rs-1722733/v1

Abstract

The present work analyzes the production and characterization of cellulose micro/nanofibers (CMNFs) obtained from different treatments. A chemical pre-treatment was performed using oxalic acid at 25 wt.% and 50 wt.%. Besides, a rotary homogenizer or a PFI mill refiner were used for mechanical pretreatments. Then, mechanical fibrillation to obtain CMNFs was performed by pressurized homogenization for 5 and 15 passes. The carboxylation of cellulose by the chemical pre-treatment was confirmed by Fourier Transform Infrared Spectroscopy (FTIR) and the increase in the carboxylic acid group content was determined by conductometric titration of CMNFs. The best results of nanofibrillation yield (76.5%), transmittance (72.1%) and surface charges (71.0 μeq/g CMNF) were obtained using the PFI mill refiner, 50 wt.% oxalic acid and 15 passes. The highest aspect ratio (length/diameter) determined by Transmission Electron Microscopy (TEM) was found using the PFI mill refiner and 25 wt.% oxalic acid treatment, and no significant differences were observed by increasing the number of passes. The aspect ratio was related to the sedimentation and the intrinsic viscosity of the CNMF dilute suspension. The aspect ratio values obtained by sedimentation agree with those of TEM. Moreover, a strong relationship between the intrinsic viscosity [η] of the CMNF dispersions and their aspect ratio (p) was found ($\rho[\eta] = 0.014\ p^{2.3}$, $R^2 = 0.99$). Finally, the tensile strength of films obtained from CMNF suspensions was more influenced by the amount of CMNF fraction than the aspect ratio.

1. Introduction

The depletion of petroleum products and the need to reduce the carbon footprint promote the development of new biodegradable materials obtained from renewable sources. Cellulose is the most abundant natural polymer that can provide rational solutions to these problems. In the last decades, the production of nanocellulose obtained from the cell walls of wood fibers and plants has gained great interest due to its interesting properties, such as high tensile strength and stiffness, low weight, renewability, biocompatibility, biodegradability and non-toxicity (Siró and Plackett 2010; Habibi et al. 2010; Xie et al. 2018).

Cellulose nanofibers (CNFs) are produced by applying an intense mechanical treatment, in which the fibers are subjected to great shearing forces that fibrillate and release microfibrils. The most common mechanical treatments include repeated steps in high-pressure homogenizers, microfluidizers, colloid mills and twin-screw extrusion (Xie et al. 2018). In general, a mechanical, chemical or enzymatic pre-treatment of fibers is necessary with the aim to partially separate them and prevent clogging, as well as to reduce the energy consumption in the homogenizer (Xie et al. 2018; Tarrés et al. 2020).

Among mechanical pre-treatments, PFI refiners were found to produce high internal fibrillation, facilitating the subsequent mechanical treatment (Ang et al. 2019). Ultra-turrax stirring can also be used as a mechanical pre-treatment to improve nanofibrillation yields and their dispersibility (Eyholzer et al. 2010; Ramos Aragão Melo et al. 2020).

2,2,6,6-Tetramethylpiperidine-1-oxyl (TEMPO)-mediated oxidation has been widely used as a chemical pre-treatment to obtain highly fibrillated CNFs (Saito et al. 2006; Besbes et al. 2011; Mishra et al. 2012). However, this reagent is very expensive and its disposal has environmental impact. Sanchez-Salvador et al. (2021) reported that TEMPO and NaBr can be reduced by 67%, without altering the properties of the CNFs by reusing reagents in the oxidation of cotton and eucalyptus cellulose; however, the cost of the reagent is also high and their disposal causes environmental concern.

Therefore, it is important to analyze in detail other chemical pretreatments. One alternative is the use of organic dicarboxylic acids, such as oxalic acid. The treatment with these reagents produces carboxylic groups through Fischer-Speier esterification of one carboxylic group on the accessible surface of the cellulose (Ji et al. 2013; Chen et al. 2016). Oxalic acid has some advantages: it is cheap, it can be recovered and corrosion in equipment is controllable (Xie et al. 2018). Chen et al. (2016) obtained CNFs using oxalic acid at different concentrations, temperatures and reaction times. CNFs showed high thermal stability and a high aspect ratio, suggesting that they could be used as bio-composites in different applications.

The use of different methods to obtain nanocellulose produces a wide range of types of cellulose micro/nanofibers (CMNFs). In general, heterogeneous mixtures of cellulose microfibers (CMFs) and CNFs are obtained. Some characteristics of CMNF suspensions, such as nanofibrillation yield, charge density and aspect ratio, are important to determine their potential applications.

The diameter of the CNFs can be determined by Atomic Force Microscopy (AFM), Scanning Electron Microscopy (SEM), and Transmission Electron Microscopy (TEM), but the length and, therefore, the aspect ratio are more difficult to assess due to entanglements of nanofibers (Zhang et al. 2012). There are different methods to estimate the aspect ratio of CNFs. Varanasi et al. (2013) proposed the sedimentation method, which is based on the gel-point concentration. The gel point is the threshold consistency at which a continuous network of fibers in suspensions is formed. This method is an adaptation of the method proposed by Martinez et al. (2001) for wood pulp fibers. Another method involves the measurement of the intrinsic viscosity of CMNF suspensions. Albornoz-Palma et al. (2020) found a relationship between this rheological parameter and the aspect ratio of enzymatic CNFs in a diluted regime.

Despite of the existing knowledge about CMNFs based on dicarboxylic acid (Chen et al. 2016; Jia et al. 2017; Luo et al 2018), to our knowledge, they have not been properly characterized. Particularly, the correlation of the aspect ratio with the shear viscosity of the CMNF dilute suspension can be very useful.

In this paper, the effect of different alternatives to obtain CMNFs was investigated. For this purpose, a chemical pre-treatment using oxalic acid at two concentrations (25 wt.% and 50 wt.%), and two mechanical pre-treatments a rotary homogenizer type ultra-turrax and a PFI mill refiner were analyzed. For the final mechanical treatment, two numbers of passes through the pressurized homogenizer (5 and 15) were considered. Carboxylation of cellulose by the chemical pretreatment and the total charges of CMNFs were determined by FTIR and conductometric titration, respectively. The obtained CMNFs were

characterized by measuring nanofibrillation yield, transmittance and surface charge. The microfibrillar and nanofibrillar fractions were observed by measuring dimensions by SEM and TEM, respectively. The aspect ratio of the nanofibrillar fraction was related to two parameters of the CMNF suspension: gel point by sedimentation and intrinsic viscosity. Finally, the tensile strength of films obtained from CMNF suspensions was analyzed.

2. Materials And Methods

2.1. CMNF preparation

CMNFs were obtained from industrial bleached eucalyptus pulp (BEP) supplied by Suzano Papel e Celulose S.A. (Brazil). The pulp was soaked in water for 24 h and disintegrated for 5 min at 1.5 wt.% consistency in water. Then, the water content of pulp was removed by centrifugation and pulp was stored at a low temperature (4°C) until use. The average dimensions of the hardwood fibers determined by optical microscopy were

15.6 μm in diameter and 0.95 mm in length.

2.1.1. Chemical pre-treatment

The chemical pre-treatment was carried out according to the technique described by Chen et al. (2016). In brief: 15 g of pulp were added to a reactor containing 750 ml oxalic acid considering two concentrations: 25 wt.% and 50 wt.%. The reaction was made at 90°C for 1h under constant stirring at 250 rpm. After that, the solution was filtered and the pulp was washed, starting with hot water to avoid the crystallization of the acid, and then, with water at room temperature. The washed step was made up to a conductivity of 20 μS/cm of the washing water. Finally, the pulp was neutralized to pH 7.0 with NaOH solution, in order to obtain the sodium form of the carboxyl groups of the pulp.

2.1.2. Mechanical pre-treatment

The fibers chemically treated with oxalic acid were treated with a rotary homogenizer type ultra-turrax (Unidrive x1000, Alemania) at 0.75% consistency in distilled water, for 3 min/g fiber at 15,000 revolutions.

On the other hand, a group of CMNFs was obtained by refining the fibers through a PFI mill at 10,000 revolutions and 10% of consistency in accordance with SCAN-C 18:65 standards. After the first 4000 revolutions, refining was interrupted to remix the pulp. Later, pulp was chemically pre-treatment (explained in section 2.1.1).

2.1.3. Mechanical Fibrillation

In all cases, the pulp was homogenized at 0.75% consistency through pilot scale pressurized homogenizer (SIMES S.A, Santa Fe) at 300 Bar, using five and fifteen steps. The CMNFs obtained were refrigerated at 4°C until they were used.

Table 1 shows the nomenclature used according to the preparation stages.

Table 1
Nomenclature of cellulose micro/nanofibers according to the treatment

Samples	PFI mill refining (revolutions)	Oxalic acid (wt.%)	Homogenizer type ultra-turrax, 3 min/g fiber (rpm)	Homogenization at 300 bar (passes)
25ox_Ut_5P	—	25	15,000	5
25ox_Ut_15P	—	25	15,000	15
50ox_Ut_5P	—	50	15,000	5
50ox_Ut_15P	—	50	15,000	15
R_25ox_5P	10,000	25	—	5
R_25ox_15P	10,000	25	—	15
R_50ox_5P	10,000	50	—	5
R_50ox_15P	10,000	50	—	15

2.2. Characterization of CMNFs

Before all characterization techniques, the CMNF solutions were sonicated for 2 minutes using a Sonics & Materials ultrasonic homogenizer (500 W, 40% amplitude) to ensure their adequate dispersion.

2.2.1. Esterification and carboxylation degree

Cellulose carboxylation by the oxalic acid treatment was identified by Fourier Transform Infrared (FTIR) spectroscopy system (Shimadzu FTIR- 8000 Spectrometer). Samples of original fibers and CMNF films were triturated and mixed with potassium bromide (KBr), and then, they were pressed into tablets. The spectra were recorded at the wavelength range of 400–4000 cm^{-1} with a resolution of 8 cm^{-1}. Each sample was scanned 40 times.

The carboxylic group content of the bleached eucalyptus pulp (BEP) and CMNFs obtained by 25 wt.% and 50 wt.% of oxalic acid treatment were determined by conductometric titration. For the original pulp, the technique proposed by Katz et al. (1984) was used. For the CMNFs, the determinations were made in a similar way to the method described by Ovalle-Serrano et al. (2018): A suspension was prepared by mixing 50 mg of CMNF in 400 mL of water. The pH was adjusted to 3.0 by adding 0.01M HCl solution to ensure a complete protonation of carboxyl groups. Conductometric titrations were performed using 0.01M NaOH as titrant under nitrogen atmosphere.

2.2.2. Nanofibrillation yield, transmittance and surface charges

The yield of nanofibrillation was determined by centrifuging (4000 rpm, 2809 g) an aqueous suspension of 0.14 wt.% CMNF for 20 min according to Schnell et al. (2018). The dry weight of the supernatant, called nanofibrillated fraction (CNF) was obtained from the difference between the initial weight (W_i) and the centrifugation sediment (W_f) which was considered as micro fibrillated fraction (CMF) (Eq. 1):

$$Yield(\%) = \left[1 - \frac{W_f}{W_i}\right] * 100$$

1

Transmittance readings of 0.1 wt.% CMNFs suspensions were performed at 800 nm using CECIL 3055 spectrophotometer and distilled water as a reference.

Surface charges of CMNFs were determined by polyelectrolyte titrations using streaming current measurements (Chemtrac ECA equipment, USA). A solution of 0.3 meq/L of cationic polyelectrolyte, poly(diallyldimethylammonium chloride) (M_w 400,000- 500,000 g/mol) from Sigma Aldrich was used as titrant. The pH of CMNF suspensions (0.04 wt.% of consistency dissolved in 1mM NaCl solution) were previously adjusted to 7.0.

2.2.3. Morphologies

Measurements of diameter and length distributions by microscopy

The diameter and length distributions of CMNF fraction of a wide greater than 1 µm were obtained by optical microscopy (Leica Microsystems Instrument). Samples were diluted to 0.1 wt.%, and a single drop of the suspension was cast on a glass support and dried at room temperature. Then, 500 diameter and 50 length measurements were made using, for both, 40X and 100X lens.

The diameter distributions of microfibrillated fraction (CMF) were examined using a Phenom Pro scanning electron microscope (SEM) (Netherlands) at accelerating voltages of 5 KV and 10 KV, with a working distance of 2.5 ± 0.5 mm. The nanofibrillated fraction was removed by centrifugation, and the sediment was used for preparing suspensions of approx. 0.015 wt.%. The suspension was sonicated, lyophilized and the swollen CNF film formed was coated with gold. More than 75 diameter measurements were made using Image J processing software. The length measurement were not possible because the high entanglement of fibers.

The diameter and length distributions of nanofibrillated fraction (CNF) were determined by transmission electron microscopy (TEM) (JEOL, JEM-2100 Plus). Observations were made in HRTEM mode, with an acceleration voltage of 100 kV. The nanofibrillated fraction was removed by centrifugation as indicated

above in section 2.2.2. An aliquot of 0.001 wt.% of CNF suspensions was mounted on a glow-discharged carbon coated Cu grid. A number of 300 diameters and 75 length measurements were performed using Image J processing software.

Sedimentation

According to the method proposed by Varanasi et al. (2013), different concentrations of CMNFs were prepared (from 0.01 to 0.07 wt.%), the suspensions were stirred for 5 min and poured into graduated cylinders to reach an original suspension height (h_0). After 48 hours, the height of sediment in the cylinder (h_s) was measured. The initial solid concentrations of CMNFs (C_0) were plotted versus (hs/h_0) and the data were adjusted to a quadratic equation. Then, the first derivate of the curve at the y-intercept gives the gel point (C_c). For this method, the density of the cellulose nanofibers was assumed 1,500 kg/m^3. Then, the aspect ratio (A) can be estimated using Crowding Number theory (CN) with the following equation:

$$A = 6\ C_c^{-0.5} \quad (2)$$

This theory considers that the CNF are shaped like straight cylinders.

Shear viscosity

The dynamic viscosity of different CMNFs was determined using a Brookfield viscometer LVT with an Ultra Low Adapter (ULA) spindle similar to the method proposed by Albornoz-Palma et al. (2020). In brief: Viscosity measurements were made at different concentrations (from 0.01 to 0.1wt. %) and shear rate of 73.38 s^{-1}. In all cases, samples were conditioned in a thermostatic bath at 25°C for 1 h, and then, they were shaken for 1 min in a vortex before the measurement.

The critical concentration (C^*) was obtained from the changes in specific viscosity as a function of the concentration of the CMNFs according to Tanaka et al. (2014).

The intrinsic viscosity [η] was obtained in the dilute region extrapolating the linear fit to a zero concentration.

2.3. Film formation from CMNFs

The formation of films was performed by adding 14 g of suspension of CMNFs at 0.75% consistency in a petri dish. The samples were dried at 30°C for 24 h. The thickness of the films was measured using a precision of 0.001 mm micrometer and the average of 10 measurements of different parts of the film was reported. The mechanical properties of the films of CMNFs were measured using INSTROM 3340 equipment with a 100 N cell. First, the film was conditioned at 23°C and 50%RH and then, 5 mm wide specimens were cut. For the mechanical tests, the ASTM D882 standard was followed. The initial distance between the grips was 22 mm and the tensile speed was 2 mm/min.

3. Results And Discussion

3.1. CMNF characterization

3.1.1. Esterification and carboxylation degree

Figure 1a shows the chemical structure of original BEP fibers and CMNFs pretreated with PFI refiner and 25 wt.% and 50 wt.% of oxalic acid analyzed by FTIR spectrophotometer. The spectra of the samples show the same cellulose characteristic peaks in 3380 cm^{-1} and 2898 cm^{-1} regions, attributed to the stretching vibration of hydroxyl groups (O-H) and the symmetric C–H stretching vibration, respectively (Tripathi et al. 2017; Luo et al. 2019). The peaks around 1640 cm^{-1} can be attributed to O–H bending vibration and the peak at 899 cm^{-1} can be assigned to β-glycosidic linkages of glucose ring in cellulose (Ganan et al. 2004; Jia et al. 2017). For the samples of CMNFs obtained by 25 wt.% and 50 wt.% oxalic acid treatment, a new weak peak was observed at 1737 cm^{-1}, corresponding to the C = O ester vibrational stretching band (Jia et al. 2017). This esterification can be attributed to the reaction between the hydroxyl group on the cellulose chains and the carboxyl group of oxalic acid through Fischer–Speier esterification of one carboxyl group of oxalic acid (Fig. 1c).

On the other hand, Fig. 1b shows the carboxyl content obtained by conductometric titration of the bleached eucalyptus pulp (BEP) and the CMNFs pre-treated with PFI refiner and with 25 wt.% and 50 wt.% oxalic acid. The total charge of CMNFs is expected to remained unaltered by mechanical treatments. Junka et al. (2013) showed that the total charge of CNFs is independent of the number of passes through a microfluidizer. The results show that there is an important increase of the carboxyl group content for both CMNFs, also confirming the carboxylation of cellulose.

3.1.2. Nanofibrillation yield, transmittance and surface charge

Table 2 shows the nanofibrillation yield, the transmittance and the surface charges of different CMNFs. The CNMFs corresponding to PFI refining pre-treatment had higher nanofibrillation yields, transmittance and surface charge than those obtained with a rotary homogenizer. Importantly, the refining step was carried out before the chemical pre-treatment because after oxalic acid treatment, the obtained paste cannot withstand a PFI refining. The mechanical pre-treatment prior to the chemical one, could have improved the accessibility between the hydroxyl groups of the cellulose and the carboxylic groups of the oxalic acid, thus increasing the nanofibrillation yield, transmittance and surface charge of the obtained CMNFs.

In addition, a significant increase in nanofibrillation yield was observed when the concentration of oxalic acid was increased from 25 wt.% to 50 wt.%. This result can be attributed to the new carboxylic groups introduced during the chemical treatment, which produce repulsive forces that facilitate the defibrillation of cellulose during the mechanical process (Sanchez-Salvador et al. 2020). Moreover, when the number

of passes of the pressurized homogenizer was increased (from 5 to 15), no significant change in nanofibrillation yield was observed, except for the pulp treated with PFI and 50 wt.% oxalic acid (from 54.3–76.5%). This result could be associated with the working relatively low pressure (300 bar) of the homogenizer compared to those normally used (900–1000 bar), which hindered the increment in the main fibrillation.

On the other hand, Table 2 also shows that the transmittance values of the CMNF suspensions were similar and low for pulps treated with the rotary homogenizer (from 8.4 to 14.5). However, for PFI refiner CNMFs, transmittance increased when the number of homogenizer passes and the concentration of oxalic acid were increased (from 18.7 to 72.1%). This increment is in agreement with a reduction in the residual fiber content and an increase in the content of optically inactive nanofibrils (higher nanofibrillation yield) in the CMNF suspensions. In addition, higher surface charges induce better stability and, therefore, higher transmittance (Jia et al. 2017, Luo et al. 2018).

The highest surface charge content was achieved for PFI refining and 50 wt.% oxalic acid treatment, reaching a value of 72.9 µeq/g CMNF. Surface charges represent the anionic nature of the fibers and have been traditionally used to determine the degree of delamination of the pulp fibers for papermaking after disintegration (Sanchez Salvador et al. 2020).

Table 2
Nanofibrillation yield, transmittance and surface charge of CMNFs

CMNF	Nanofibrillation yield (%)[a]	Transmittance (800 nm) (%)	Surface charge (µeq/g CMNF)[a]
25ox_Ut_5P	4.5 ± 1.2	14.5	10.3 ± 0.9
25ox_Ut_15P	5.1 ± 1.6	10.6	11.8 ± 0.1
50ox_Ut_5P	19.5 ± 1.4	8.4	18.5 ± 2.1
50ox_Ut_15P	20.6 ± 1.6	10.1	30.5 ± 1.5
R_25ox_5P	11.6 ± 1.2	18.7	19.6 ± 1.9
R_25ox_15P	12.8 ± 1.8	22.4	21.7 ± 0.2
R_50ox_5P	54.3 ± 0.33	48.3	72.9 ± 0.3
R_50ox_15P	76.5 ± 0.28	72.1	71.0 ± 0.6

[a] Values are the average of two replicates of the trial

3.1.3. Morphologies

Measurement of diameter and length distributions by microscopy

The CMNFs obtained with the different treatments were heterogeneous, i.e., they present an ample wide size range. In this work, we analyzed three fractions: a) wide greater than 1 μm, b) microfibrillar (CMF) and c) nanofibrillar fractions (CNF).

Table 3 shows the results of average diameter, length and aspect ratio of CMNF fraction of a wide greater than 1 μm determined by optical microscopy (OM). The average diameter values were similar (from 10.7 μm to 11.9 μm) when the rotary homogenizer was used, irrespective of the chemical treatments applied. For pulps refined by PFI mill, the average diameter values were lower (from 2.1 to 3.9 μm). In addition, Table 3 shows that the average length and the aspect ratio decreased with increasing oxalic acid concentration in the chemical treatment. The same effect was observed with the number of pressurized homogenizer passes, for both the rotatory homogenizer and refining process. The highest aspect ratio was obtained for R_25ox_5P treatment. Figure 2 shows the OM images and histograms of length and diameter of samples 25ox_UT_5P and R_50ox_15P. A strong morphological difference is observed between these mechanical treatments. For the rotary homogenization process, cut fibers are observed, whereas for the refining process, slender shavings are observed, indicating a fibrillation effect.

Table 3
Average diameter, length and aspect ratio of original pulp and CMNF fraction of a wide greater than 1 µm determined by optical microscopy (OM)

CMNF	Average diameter (µm)[a]	Average length (µm)[b]	Average aspect ratio (length/diameter)
BEP	15.6 ± 4.0	945.3 ± 271.4	60.4
25ox_UT_5P	11.9 ± 4.5	63.9 ± 17.2	5.4
25ox_UT_15P	10.6 ± 3.3	42.6 ± 14.9	4.2
50ox_UT_5P	10.9 ± 3.4	32.0 ± 7.8	2.9
50ox_UT_15P	10.7 ± 3.3	29.1 ± 7.2	2.7
R_25ox_5P	3.9 ± 3.6	48.7 ± 28.4	14.1
R_25ox_15P	3.3 ± 2.5	25.6 ± 13.3	7.8
R_50ox_5P	2.8 ± 1.0	11.1 ± 5.5	4.0
R_50ox_15P	2.1 ± 1.0	7.7 ± 2.7	3.6
[a] Values are the average of 500 measurements			
[b] Values are the average of 50 measurements.			

Images and diameter histograms of the CMF determined by SEM are shown in Fig. 3. The presence of entangled microfibers was observed; therefore, it was not possible to measure their length, since their beginning and end were undistinguishable. In addition, some lamella and branches were observed, and both elements suggest that the mechanical treatment has not been sufficient to finish separation of the microfibrils. The average diameters of all CMFs were very similar (from 179 ± 43 nm to 257 ± 69 nm). The diameter histograms of all CMFs are shown in Fig. S1 in the Supplementary material.

Table 4 shows average diameter, length and aspect ratio of cellulose nanofiber fraction (CNF) determined by TEM. No significant differences were observed in the average diameters of any of the CNFs (from 12 ± 3.0 nm to 16 ± 4.8 nm). However, a decrease in the average lengths was observed for 50% oxalic acid treatment (approx. 725 nm) compared to those obtained by 25% oxalic acid treatment (approx. 1250 nm). This result indicates that the chemical pre-treatment with higher concentration of oxalic acid reduced the length of the CNFs, generating a decrease in their aspect ratio.

In addition, pulps treated with PFI showed a higher aspect ratio than those treated with the rotatory homogenizer, and the number of pressurized homogenizer passes did not influence the morphology of the CNFs obtained. Figure 4 shows the TEM images and histograms of CNF samples 25ox_UT_5P and R_50ox_15P, respectively.

Table 4
Average diameter of CNF determined by TEM

CNF	Average diameter CNF (nm)[a]	Average length (nm)[b]	Average aspect ratio (length/diameter)
25ox_Ut_5P	16.0 ± 5.0	1262 ± 443	78.9
25ox_Ut_15P	16.0 ± 4.8	1250 ± 430	78.0
50ox_Ut_5P	12.0 ± 3.0	725 ± 248	60.4
50ox_Ut_15P	12.6 ± 3.7	727 ± 322	57.7
R_25ox_5P	12.5 ± 4.2	1204 ± 298	96.3
R_25ox_15P	13.2 ± 3.5	1298 ± 569	98.3
R_50ox_5P	12.0 ± 3.5	793 ± 227	66.1
R_50ox_15P	12.5 ± 3.0	707 ± 183	56.6
[a] Values are the average of 300 measurements.			
[b] Values average of 75 measurements.			

Sedimentation

Figure 5 shows initial concentrations of CMNFs as a function of the ratio of initial (h_o) to final height (h_s) of CMNF after 48 h. Data were fitted with a quadratic equation. The first derivative of the curve at the y-intercept gave the gel point (C_c) and the aspect ratio (A) was estimated using Eq. (2) (Table 5). For CMNFs corresponding to 25 wt.% oxalic acid, aspect ratio did not change with increasing number of passes through the homogenizer. In addition, the CNMF obtained by PFI mill shows a higher aspect ratio than the CNMF obtained by rotary homogenizer. The aspect ratio indicated by sedimentation gel point agrees with those measured by TEM **(**Table 4). It should be noted that, for the sedimentation procedure, both the microfibrillar (CMF) and the nanofibrillar (CNF) fractions were involved, but for TEM, only nanofibrillar (CNF) fractions were considered. This result can be explained by the existence of a similar aspect ratio between the microfibrillar and nanofibrillar fractions. Results indicate that a simple technique such as sedimentation can be used to estimate the aspect ratio of these CNFs.

However, this technique has some limitations, since the final height of sedimentation cannot be always observed. This occurred for the CMNFs obtained by 50 wt.% oxalic acid treatment, which has a higher

content of carboxylic groups and, therefore, higher repulsive forces can prevent their agglomeration and sedimentation.

Sanchez Salvador et al. (2020) analyzed the effect of the stability reduction of a CNF suspension and the decrease in a gel point, by changing the pH and the salt concentration of the medium. For this purpose, a CNF of high-charge obtained with a pre-treatment with TEMPO-mediated oxidation was used. They showed that, with the pH value under 4.8 (corresponding to the value of the pk_a of COO^-) and at a high salt concentration (≥ 5 mM $CaCl_2$), the charges decreased and the electrical double layer was compressed, respectively.

Table 5
Sedimentation data fitted with a quadratic equation, gel point (C_c) and aspect ratio (A) of CMNFs according to CN theory

CMNF	$Y = Ax^2 + Bx$ (*)	Gel point (C_c) (wt.%)(**)	Aspect ratio (A) (length/diameter)
25ox_Ut_5P	$y = -1.861x^2 + \mathbf{0.794}x$	0.794	67.3
25ox_Ut_15P	$y = 10.99x^2 + \mathbf{0.793}x$	0.793	67.4
R_25ox_5P	$y = 0.178x^2 + \mathbf{0.361}x$	0.361	99.9
R_25ox_15P	$y = -0.044x^2 + \mathbf{0.401}x$	0.401	94.8
*R^2 higher than 0.99 for all case, where Y is initial solid concentration and X is $(h_s)/(h_0)$			
**The first derivate of the curve at the y-intercept gives the gel point (C_c)			

Shear viscosity

The aspect ratio was also associated with the intrinsic viscosity of the suspension. Under dilute condition, the interactions between CNMFs were not significant and the rheological properties depended mainly on the morphology of the CNMFs and their entanglements (Morris et al. 1981, Albornoz-Palma et al. 2020). The dilute region is determined by identifying the change in specific viscosity (η_{sp}) as a function of the concentration of CNFs in the dispersion (Morris et al. 1981). Besides, the dilute region (Newtonian behavior) and another semi-dilute region above the critical concentration (C^*) (power-law region) can be identified (Haward et al. 2012; Albornoz-Palma et al. 2020).

Figure 6a shows the plot of specific viscosity (η_{sp}) as a function of concentration for 25ox_UT_5P. It is observed that the *C** is clearly defined. The *C** values of all CMNFs are shown in Fig. S2 in the Supplementary material. Table 6 shows critical concentration (*C**) values of all CMNFs here considered. The 50 wt.% oxalic acid CMNFs dispersions had a higher critical concentration than 25 wt.% oxalic acid ones. This result can be attributed to the higher quantity of charges incorporated in the chemical pre-treatment. The increase in charge content generates a greater repulsion between the nanofibrils, which makes it possible to increase the dilute region (Albornoz-Palma et al. 2020). Besides, there i wasa decrease in interfibrillar interactions due to a decrease in the length of the fibrils.

A relationship between the critical concentration (*C**) and the aspect ratio (*p*) of the CNFs determined by TEM was established (Fig. 6b):

$$C^* \left[\frac{g}{ml}\right] = \frac{2.82}{p^2}$$

for aspect ratio values between 60–97. The relationship here found is in agreement with that determined by other authors. For instance, Mason (1950) found a relationship of $C^* = 1.5/p^2$ for *p*-values between 20–60 for rigid-rod fibers, and Tanaka et al. (2014) found $C^* = 18/p^2$ for *p*-values between 90–330 for CNF obtained with (TEMPO)-mediated oxidation. All the relationships show the same trend but with different slopes. It can be concluded that, as the aspect ratio of the CNFs increases, the slope of the relationship increases. Besides, Albornoz-Palma et al. (2020) analyzed a mechanical CNF with enzymatic pre-treatment and found the relationship $C^* = 67.0/p^2$ for *p*-values between 146–326. The slope of this relationship was greater than that found by Tanaka et al. (2014) for CNF obtained by chemical pre-treatment, with similar aspect ratios. They concluded that the type of pre-treatment performed (chemical, enzymatic or mechanic) on the CNF also influences the slope obtained.

Figure 7a shows the reduced viscosity ((η_{red}) as a function of concentration of the CMNF dispersions in the dilute region (Newtonian behavior). Intrinsic viscosities were obtained by extrapolating the linear fit to zero concentration. The intrinsic viscosity results are shown in Table 6. Higher intrinsic viscosity values were obtained for 25wt.% oxalic acid CMNFs compared to 50 wt.% oxalic acid ones. No significant difference was detected in the diameters of the CNFs, but their lengths decreased in the nanofibrillar fraction with increasing oxalic acid concentration (Table 4). This length reduction decreased the effective volume of CMNF suspensions, which explains the lower intrinsic viscosity. On the other hand, the 25 wt.% oxalic acid CNMFs had a lower nanofibrillation yield than 50 wt.% oxalic acid ones. It can be assumed that the nanofibrillar fraction slightly influences the viscosity when the concentration of the suspensions tends to zero. In addition, the CMNFs corresponding to PFI refiner pretreatment showed a higher intrinsic viscosity than those treated with a rotary homogenizer, for each chemical treatment applied. PFI mill CMNFs had higher surface charge, which can generates an increase in the effective volume.

Table 6
The critical concentration (C^*) and intrinsic viscosity of CMNFs dispersions

CMNF	Critical concentration (C^*) CMNF (wt.%)	Intrinsic viscosity CMNF (mL/g)
25ox_Ut_5P	0.040	187.9
25ox_Ut_15P	0.048	225.4
50ox_Ut_5P	0.079	129.1
50ox_Ut_15P	0.077	108.1
R_25ox_5P	0.029	367.6
R_25ox_15P	0.038	410.5
R_50ox_5P	0.071	145.5
R_50ox_15P	0.089	115.9

Figure 7b shows that a strong relationship can be established between intrinsic viscosity and aspect ratio ($R^2 = 0.99$):

$\rho\,[\eta] = 0.014\ p^{2.3}$

where ρ is the density of the CMNFs (1.5 g/mL) that is included to make the intrinsic viscosity dimensionless. This relationship has a higher exponential term than previous records (Tanaka et al. (2015): $\rho\,[\eta] = 0.15\ p^{1.9}$; and Albornoz-Palma et al. (2020): $\rho\,[\eta] = 0.051\ p^{1.85}$), indicating greater rigidity of the nanofibers (Tanaka et al. 2015). In addition, a smaller constant of the equation was observed. This constant is related to the nature of the type of CNFs and their configuration in the dispersion (Albornoz-Palma et al. 2020).

On the other hand, when the aspect ratio of the nanofibers increases, their flexibility increases (Switzer and Klingenberg, 2003). Flexible nanofibers subjected to shear stress produce higher hydrodynamic forces (higher viscosity) than rigid nanofiber suspensions (Tanaka et al. 2015). Therefore, it can be concluded that the nanofibers obtained with PFI refining and 25 wt.% oxalic acid have the highest aspect ratio, flexibility and, therefore, intrinsic viscosity.

Figure 8 represents the CNMF suspensions obtained by different pre-treatments. The number of steps in the pressure homogenizer is not considered because this variable shows minor effects. Results of nanofibrillation yield, surface charge, diameter and length were considered in this illustration. The pulp

treated with 50 wt.% oxalic acid had a higher amount of nanocellulose and surface charge, but shorter length than those treated with 25 wt.% oxalic acid. In addition, the pulp treated with a PFI mill refiner had a higher amount of nanocellulose, a higher amount of surface charges and a slight increase in aspect ratio than those pre-treated with a rotary homogenizer.

3.2. Film formation of CMNFs

Figure 9a shows the tensile stress-strain curve of the films formed from CMNFs. The films obtained with the rotary homogenizer were very brittle and it was not possible to test them. They were more translucent and less homogeneous (Fig. 9b, 25ox_UT_5P) than the films obtained by PFI refiner (Fig. 9c, R_25ox_5P). These physical properties may be due to lower yield of nanofibrillation of these CMNFs.

Films obtained from 50 wt.% oxalic acid CMNFs had higher tensile strength than films obtained from25 wt.% oxalic acid. This result indicates that the nanofibrillation yield has more influence on film strength than their aspect ratio.

4. Conclusions

The differences in the pre-treatments strongly influenced the characteristics of the CMNFs obtained. CMNFs obtained employing PFI refining before chemical pre-treatment had better characteristics than those obtained using the rotary homogenizer. On the other hand, 50 wt.% oxalic acid CMNFs showed higher nanofibrillation yield, transmittance, and total and surface charges, but lower aspect ratio than 25 wt.% oxalic acid ones. The increase in the number of passes through the pressurized homogenizer did not produce significant changes in the characteristics of the CMNFs. For CMNFs obtained by 25 wt.% oxalic acid treatment, aspect ratio measured by TEM agreed with that obtained with sedimentation values. On the other hand, a strong relationship between the intrinsic viscosity of the CMNF dispersions and their aspect ratio was found. Both parameters, sedimentation gel point and intrinsic viscosity, can be useful to calculate the aspect ratio of this kind of CMNFs. Finally, the tensile strength of CMNF films was more influenced by nanofibrillation yield than their aspect ratio.

Declarations

ACKNOWLEDGEMENTS

The authors wish to acknowledge<z the financial support received from: a) Agencia I+D+i (PICT 2018 Nº 4410 and PICT 2019 Nº 03246); b) ASaCTel Santa Fe - IO 2018 Nº 0299 and c) CAI+D 2020 PI, Tipo II- Nº 50620190100135LI and d) CONICET. The authors would like to thank Paulina Giancarelli for her work in the lab.

Ethics approval and consent to participate

Not applicable.

Human/animal rights

This article does not contain any studies with human or animal subjects performed by any of the authors.

Consent for publication

Not applicable.

Availability of data and materials

Not applicable.

Code availability

Not applicable.

Competing interests

The authors have no competing interests to declare that are relevant to the content of this article.

Funding

The authors have not disclosed any funding.

Author contributions

All authors contributed to the study conception and design. Material preparation, data collection and analysis were performed by Gabriela. A. Bastida, Carla N. Schnell, Paulina Mocchiutti, Yamil N. Solier, Maria C. Inalbon, Miguel A. Zanuttini and María V. Galván. María V. Galván wrote the first draft of the manuscript and all authors commented on previous versions of the manuscript. All authors read and approved the final manuscript.

References

1. Albornoz-Palma G, Betancourt F, Mendonça RT, Chinga-Carrasco G, Pereira M (2020) Relationship between rheological and morphological characteristics of cellulose nanofibrils in dilute dispersions. Carbohydr Polym 230, 115588. https://doi.org/10.1016/j.carbpol.2019.115588
2. Ang S, Haritos V, Batchelor W (2019) Effect of refining and homogenization on nanocellulose fiber development, sheet strength and energy consumption. Cellulose 26(8):4767–4786. https://doi.org/10.1007/s10570-019-02400-5
3. Besbes I, Alila S, Bouf S (2011) Nanofbrillated cellulose from TEMPO-oxidized eucalyptus fbres: efect of the carboxyl content. Carbohydr Polym, 84 (3): 975–983. https://doi.org/10.1016/j.carbpol.2010.12.052

4. Chen L, Zhu JY, Baez C, Kitin P, Elder T (2016) Highly thermal-stable and functional cellulose nanocrystals and nanofibrils produced using fully recyclable organic acids. Green Chem 18: 3835–3843. https://doi.org/10.1039/C6GC00687F
5. Eyholzer C, Bordeanu N, Lopez-Suevos F, Rentsch D, Zimmermann T, Oksman K (2010) Preparation and characterization of water-redispersible nanofibrillated cellulose in powder form. Cellulose 17(1): 19–30. https://doi.org/10.1007/s10570-009-9372-3
6. Ganan P, Cruz J, Garbizu S, Arbelaiz A, Mondragon M (2004) Stem and bunch banana fibers from cultivation wastes: effect of treatments on physico-chemical behavior. J Appl Polym Sci 94(4): 1489–1495. https://doi.org/10.1002/app.21061
7. Habibi Y, Lucia LA, Rojas OJ (2010) Cellulose nanocrystals: chemistry, self-assembly, and applications. Chemical Reviews 110(6): 3479–3500. https://doi.org/10.1021/cr900339w
8. Haward S J, Sharma V, Butts CP, McKinley GH, Rahatekar SS (2012) Shear and extensional rheology of cellulose/ionic liquid solutions. Biomacromolecules 13(5): 1688–1699. https://doi.org/10.1021/bm300407q
9. Ji H, Xiang Z, Qi H, Han T, Pranovich A, Song T (2013) Strategy towards one-step preparation of carboxylic cellulose nanocrystals and nanofibrils with high yield, carboxylation and highly stable dispersibility using innocuous citric acid. Green Chemistry 21(8): 1956–1964. https://doi.org/10.1039/C8GC03493A
10. Jia Ch, Chen L, Shao Z, Agarwal UP, Hu L, Zhu J Y (2017) Using a fully recyclable dicarboxylic acid for producing dispersible and thermally stable cellulose nanomaterials from different cellulosic sources. Cellulose 24: 2483–2498. https://doi.org/10.1007/s10570-017-1277-y
11. Junka K, Filpponen I, Tom Lindström T, Laine J (2013) Titrimetric methods for the determination of surface and total charge of functionalized nanofibrillated/ microfibrillated cellulose (NFC/MFC). Cellulose 20: 2887–2895. https://doi.org/10.1007/s10570-013-0043-z
12. Katz S, Beatson RP, Scallan AM (1984) The determination of strong and weak acidic groups in sulphite pulps. Sven Papperstidning 87: 48–53.
13. Luo J, Huang K, Xu Y, Fan Y (2019) A comparative study of lignocellulosic nanofibrils isolated from celery using oxalic acid hydrolysis followed by sonication and mechanical fibrillation. Cellulose 26: 5237–5246. https://doi.org/10.1007/s10570-019-02454-5
14. Martinez DM, Buckley K, Jivan S, Lindstrom A, Thiruvengadaswamy R, Olson JA, Ruth TJ, Kerekes RJ (2001) Characterizing the mobility of papermaking fibres during sedimentation. In: Baker CF (ed) The science of papermaking, transactions of the 12th fundamental research symposium, Oxford. The Pulp and Paper Fundamental Research Society, Bury, Lancaster, UK, pp 225–254
15. Mason SG (1950).The motion of fibers in flowing liquids. Pulp Pap Mag Can 51: 93–100.
16. Mishra SP, Manent AS, Chabot B, Daneault C (2012) The use of sodium chlorite in post-oxidation of TEMPO-oxidized pulp: Effect on pulp characteristics and nanocellulose yield. Journal of Wood Chemistry and Technology 32(2): 137–148. https://doi.org/10.1080/02773813.2011.624666

17. Morris ER, Cutler AN, Ross-Murphy SB, Rees DA, Price J (1981) Concentration and shear rate dependence of viscosity in random coil polysaccharide solutions. Carbohydr Polym 1(1): 5–21. https://doi.org/10.1016/0144-8617(81)90011-4
18. Ovalle-Serrano SA, Gómez FN, C Blanco-Tirado C, Combariza MY (2018) Isolation and characterization of cellulose nanofibrils from Colombian Fique decortication by-products. Carbohydr Polym 189:169–177. https://doi.org/10.1016/j.carbpol.2018.02.031
19. Ramos Aragão Melo A, Dutra Filho JC, Cucinelli Neto RP, Ferreira WS, Soares Archanjo B, Verdan Curti R, Bruno Tavares MI (2020) Effect of Ultra-Turrax on Nanocellulose Produced by Acid Hydrolysis and Modified by Nano ZnO by Sol-Gel Method. Materials Sciences and Applications 11: 150–166. https://doi.org/10.4236/msa.2020.112009
20. Saito T, Nishiyama Y, Putaux JL, Vignon M, Isogai A (2006) Homogeneous suspensions of individualized microfbrils from TEMPO-catalyzed oxidation of native cellulose. Biomacromolecules 7(6): 1687–1691. https://doi.org/10.1021/bm060154s
21. Sanchez-Salvador JL, Monte MC, Batchelor W, Garnier G, Negro C, Blanco A (2020) Characterizing highly fibrillated nanocellulose by modifying the gel point methodology. Carbohydr Polym 227: 115340. https://doi.org/10.1016/j.carbpol.2019.115340
22. Sanchez-Salvador JL, Campano C, Negro C, Monte MC, Blanco A. (2021) Increasing the Possibilities of TEMPO-Mediated Oxidation in the Production of Cellulose Nanofibers by Reducing the Reaction Time and Reusing the Reaction Medium. Adv. Sustainable Syt. 5 (4): 2000277. https://doi.org/10.1002/adsu.202000277
23. Schnell CN, Tarrés Q, Galván MV, Mocchiutti P, Delgado-Aguilar M, Zanuttini MA, Mutjé P (2018) Polyelectrolyte complexes for assisting the application of lignocellulosic micro/nanofibers in papermaking. Cellulose 25: 6083–6092. https://doi.org/10.1007/s10570-018-1969-y
24. Siró I, Plackett D (2010) Microfibrillated cellulose and new nanocomposite materials: a review. Cellulose 17(3): 459–494. https://doi.org/10.1007/s10570-010-9405-y
25. Switzer III LH, Klingenberg DJ (2003) Rheology of sheared flexible fiber suspensions via fiber-level simulations. Inc J Rheol 47(3): 759–778. https://doi.org/10.1122/1.1566034
26. Tanaka R, Saito T, Ishii D, Isogai A (2014) Determination of nanocellulose fibril length by shear viscosity measurement. Cellulose 21(3): 1581–1589. https://doi.org/10.1007/s10570-014-0196-4
27. Tanaka R, Saito T, Hondo H, Isogai A (2015) Influence of Flexibility and Dimensions of Nanocelluloses on the Flow Properties of Their Aqueous Dispersions. Biomacromolecules 16 (7): 2127–2131. https://doi.org/10.1021/acs.biomac.5b00539
28. Tarrés Q, Oliver-Ortega H, Boufi S, Pèlach A, Delgado-Aguilar M; Mutjé P (2020) Evaluation of the fibrillation method on lignocellulosic nanofibers production from eucalyptus sawdust: A comparative study between high-pressure homogenization and grinding. International Journal of Biological Macromolecules 145: 1199–1207. https://doi.org/10.1016/j.ijbiomac.2019.10.046
29. Tripathi A, Ferrer A, Khan SA, Rojas OJ (2017) Morphological and thermochemical changes upon autohydrolysis and microemulsion treatments of coir and empty fruit bunch residual biomass to

isolate lignin-rich micro- and nanofibrillar cellulose. ACS Sustain Chem Eng 5:2483–2492. https://doi.org/10.1021/acssuschemeng.6b02838

30. Varanasi S, He R, Batchelor W (2013) Estimation of cellulose nanofibre aspect ratio from measurements of fibre suspension gel point. Cellulose 20: 1885–1896. https://doi.org/10.1007/s10570-013-9972-9
31. Xie H, Du H, Yang X, Si Ch (2018) Recent Strategies in Preparation of Cellulose Nanocrystals and Cellulose Nanofibrils Derived from Raw Cellulose Materials. Review Article. International Journal of Polymer Science 5: 1–25. https://doi.org/10.1155/2018/7923068
32. Zhang L, Batchelor W, Varanasi S, Tsuzuki T, Wang X (2012) Effect of cellulose nanofiber dimensions on sheet forming through filtration. Cellulose 19(2): 561–574. https://doi.org/10.1007/s10570-011-9641-9

Scheme

Scheme 1 is available in Supplementary Files section.

Figures

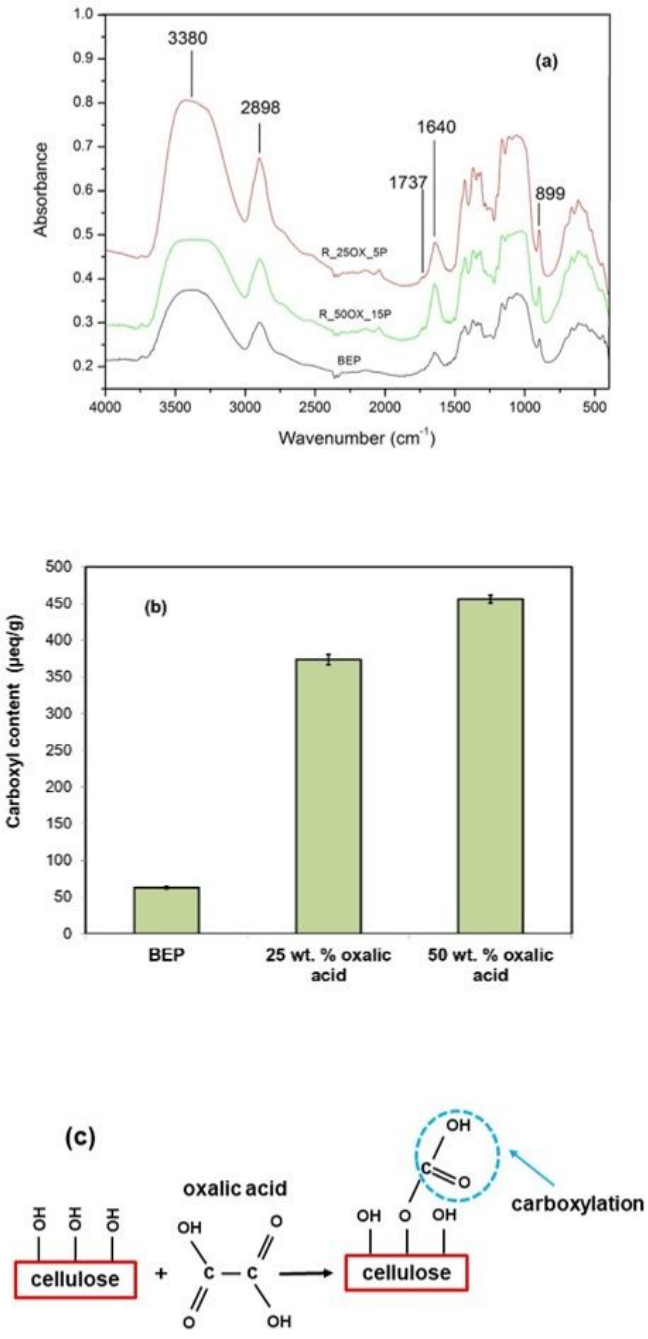

Figure 1

a FTIR spectra and **b** carboxyl content of the original bleached eucalyptus pulp (BEP) and the CMNF obtained from pulp treated with 25 wt.% and 50 wt.% oxalic acid. **c** Schematic diagram of cellulose carboxylation (*Chen et al. 2016*)

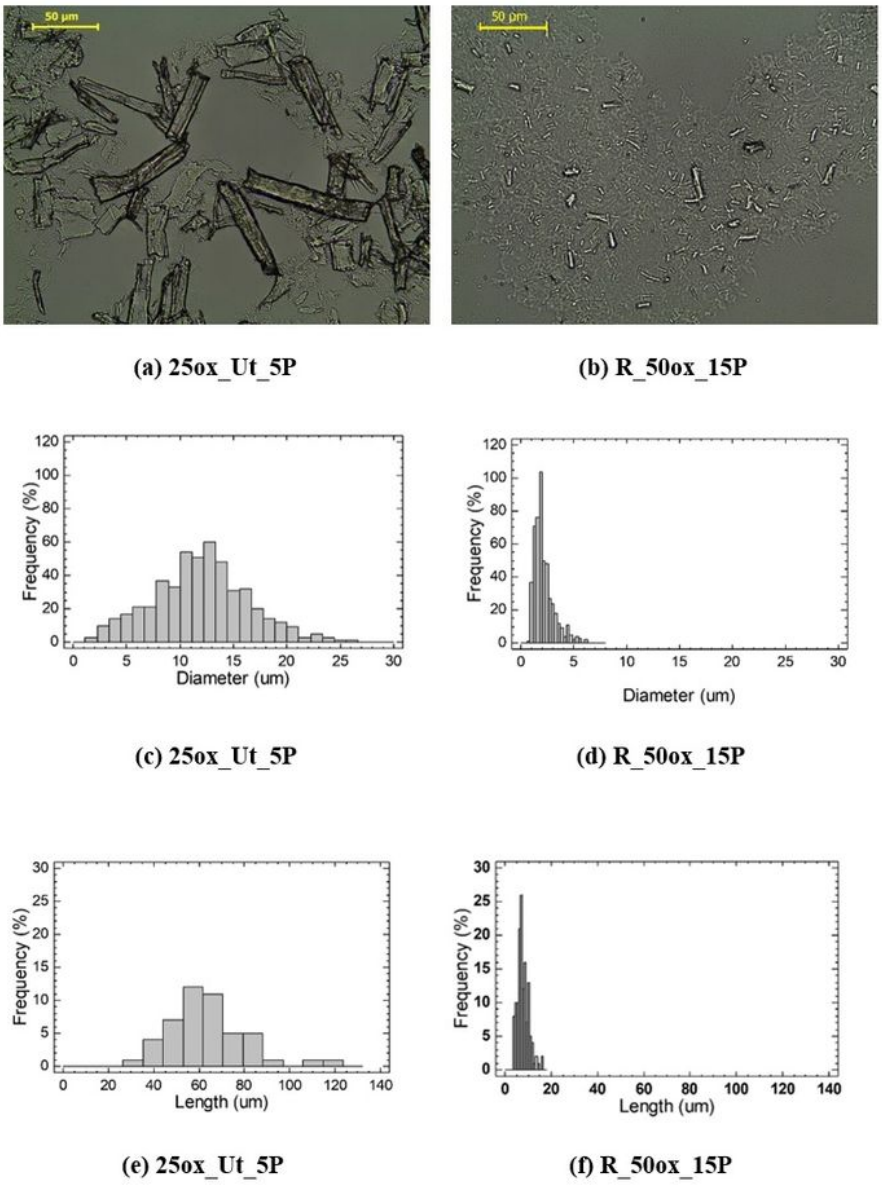

Figure 2

Optical microscopy images of (a) 25ox_UT_5P and (b) R_50ox_15P of CMNF. Distribution of diameter (c, e) and length (d, e) of samples fraction of a wide greater than 1 µm

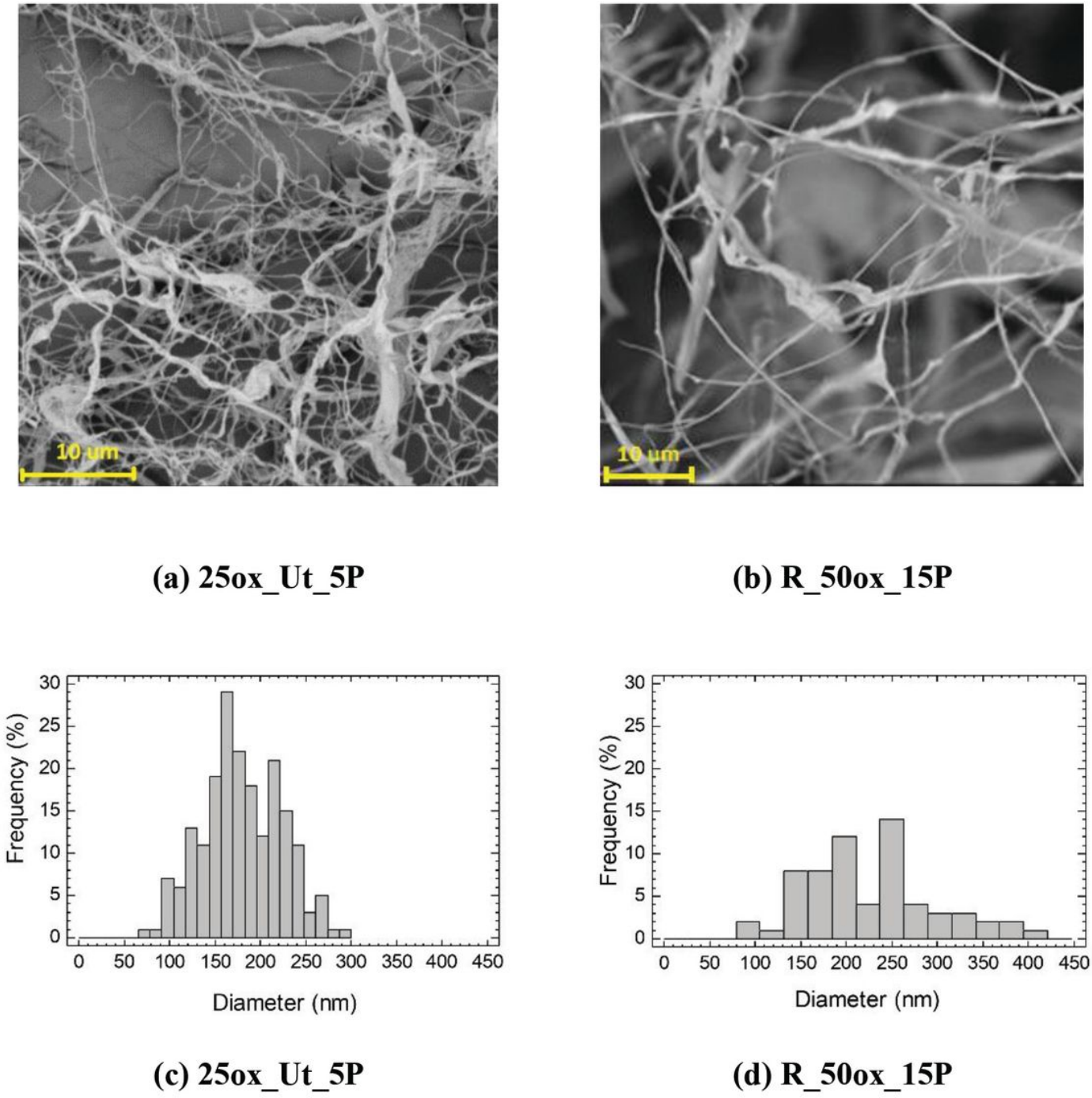

Figure 3

SEM images (scale of 10 µm) and distribution of diameter of samples 25ox_UT_5P and R_50ox_15P of cellulose microfibrillar fraction (CMF)

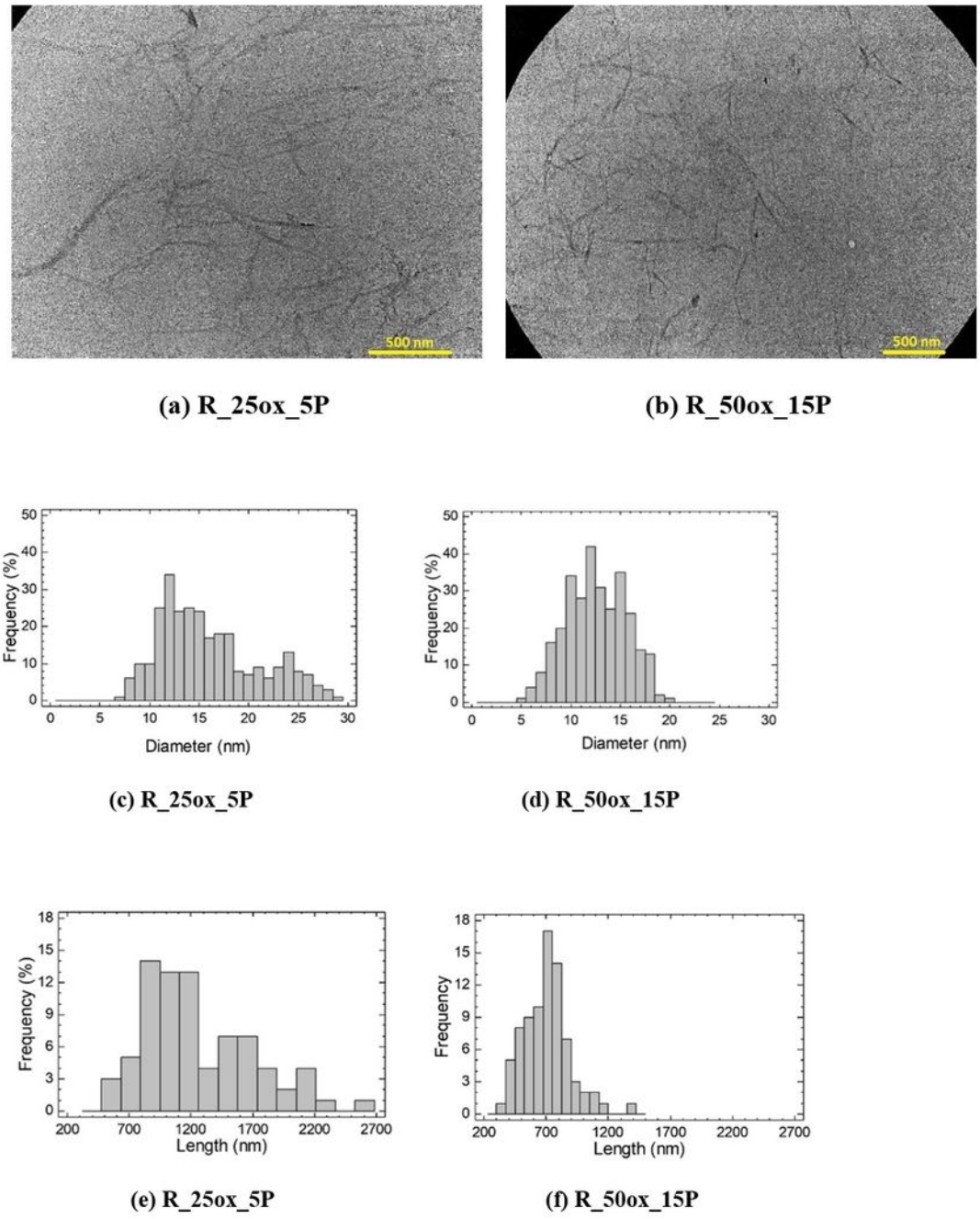

Figure 4

TEM images (scale 500 nm), distribution of diameter and length of samples 25ox_UT_5P and R_50ox_15P of cellulose nanofibrillar fraction (CNF)

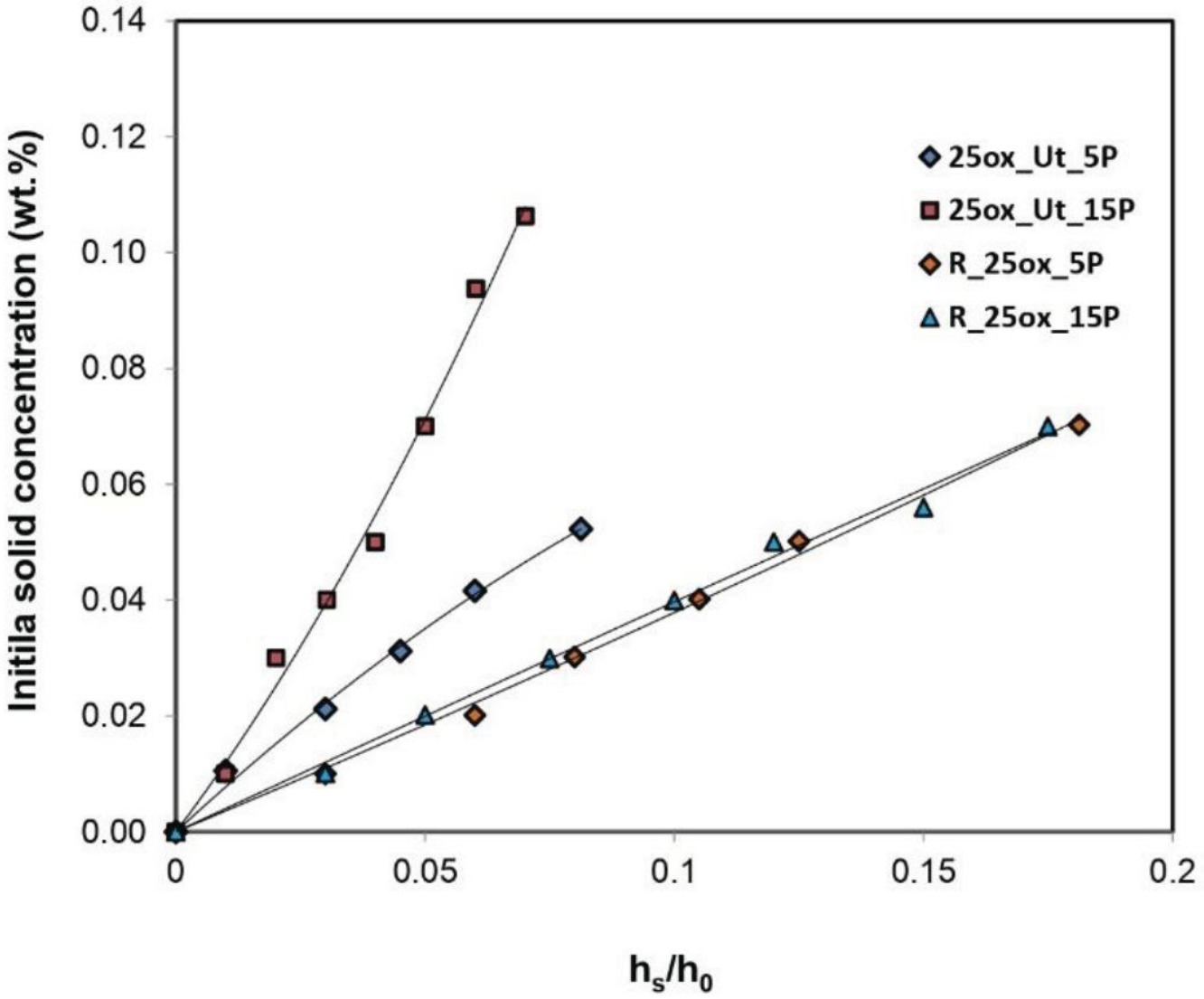

Figure 5

Initial solid concentration vs final sediment height (h_s)/initial (h_0) height of suspension

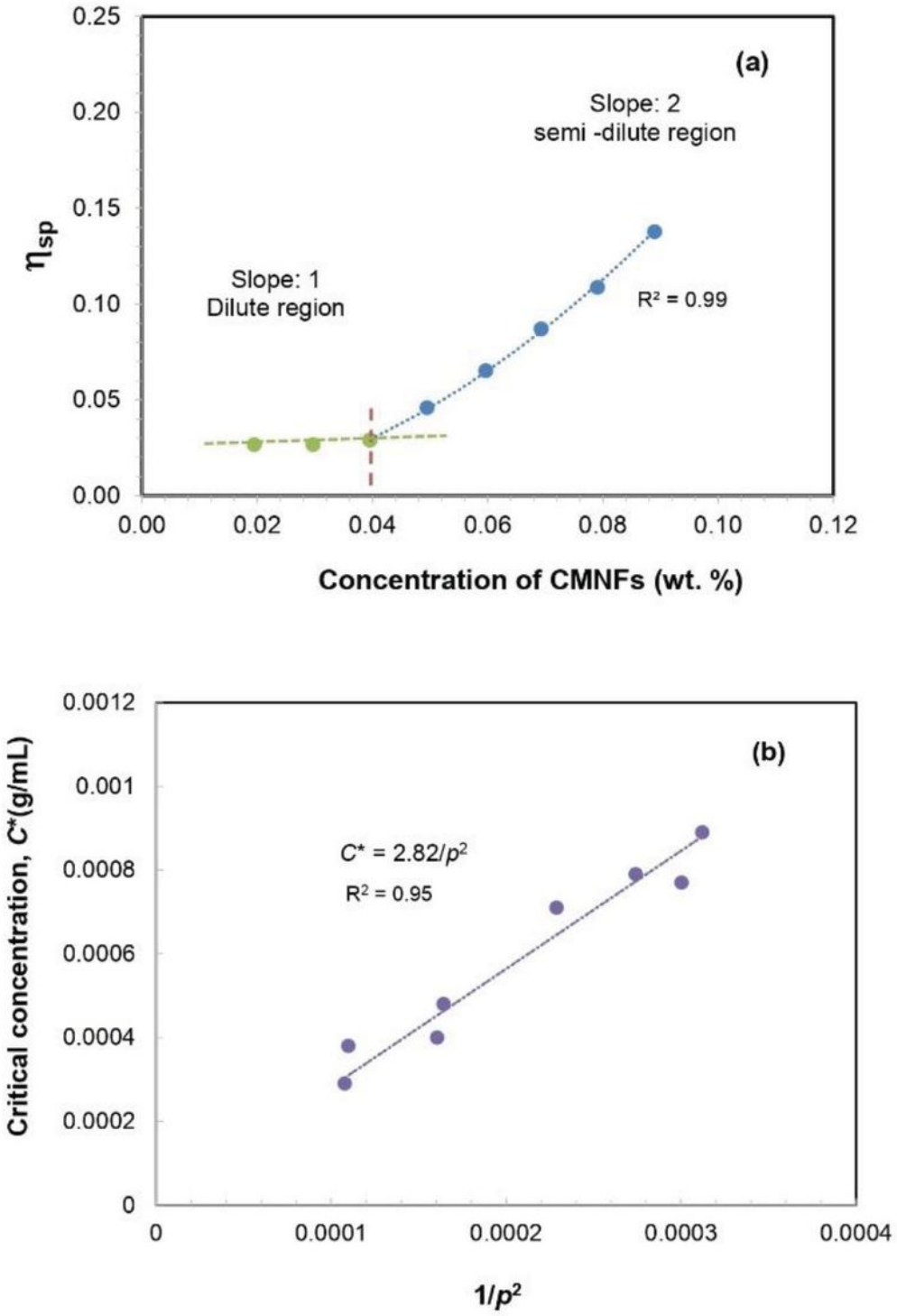

Figure 6

a Specific viscosity (h_{sp}) as a function of the concentration for 25ox_UT_5P CMNF, and **b** critical concentration (C^*) as a function of the inverse square of the aspect ratio ($1/p^2$) for all CMNFs analyzed

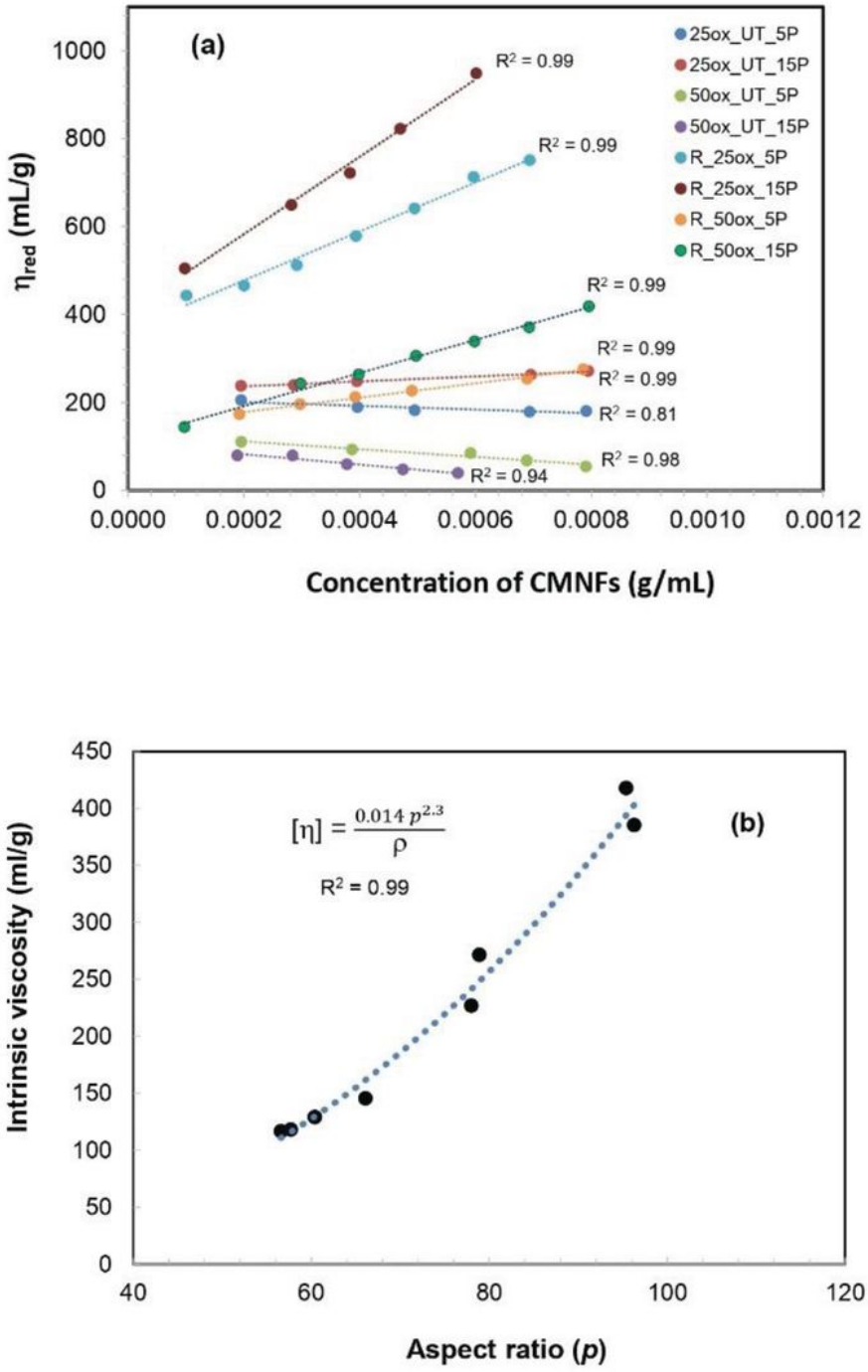

Figure 7

a Variation in the reduced viscosity according to the concentration of CMNFs in the dilute region, and **b** Intrinsic viscosity of the CMNF suspensions as a function of the aspect ratio (*p*)

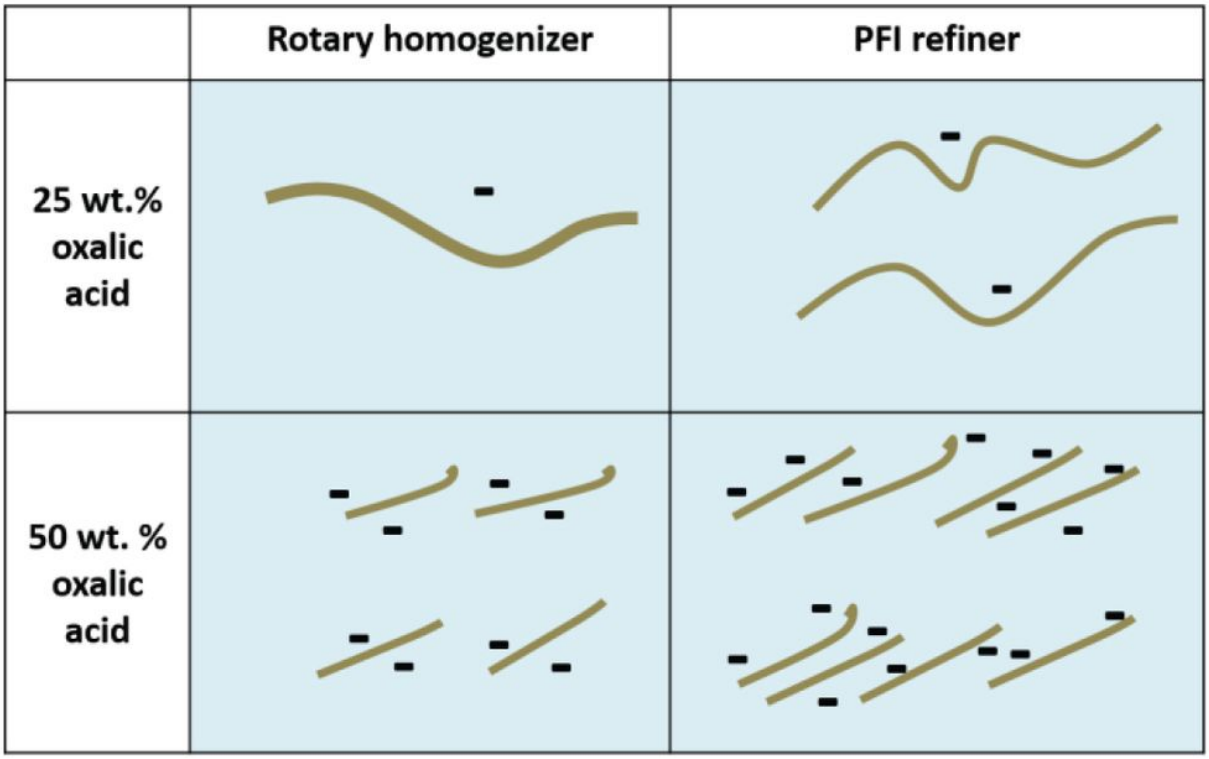

Figure 8

Schematic representation of CNF suspension obtained with different chemical and mechanical pre-treatments

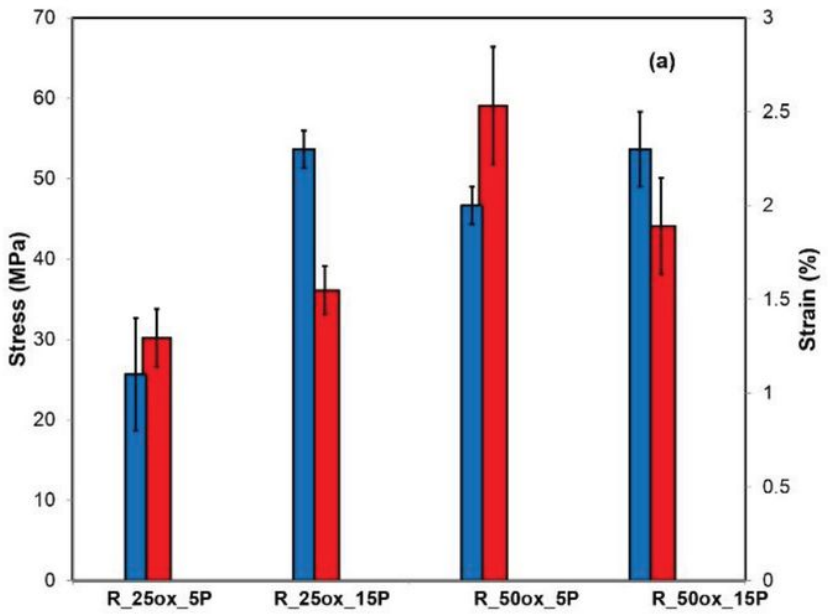

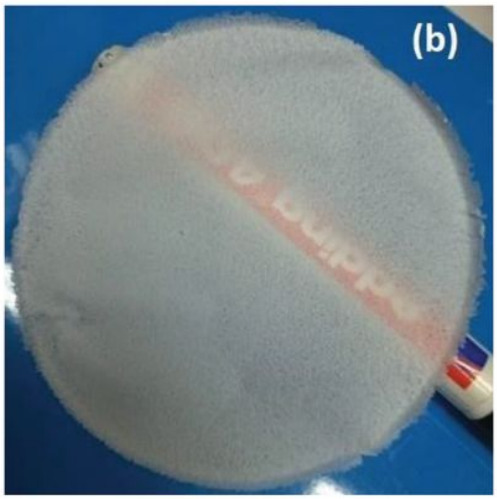

25ox_UT_5P

R_25ox_5P

Figure 9

a Stress and strain of the CNMF films, **b** and **c** photographs of 25 % oxalic acid CNMF films obtained by pre-treatments with rotary homogenizer and the PFI refiner, respectively

Supplementary Files

This is a list of supplementary files associated with this preprint. Click to download.

- sch1.jpg
- SupplementaryMaterial.docx